Advanced Powder Technology 24 (2013) 1048–1053

Contents lists available at SciVerse ScienceDirect

Advanced Powder Technology

journal homepage: www.elsevier.com/locate/apt

Original Research Paper

Structural and microstructural phase evolution during mechano-synthesis of nanocrystalline/amorphous CuAlMn alloy powders

R. Amini [a,*], S.M.M. Mousavizad [a,b], H. Abdollahpour [b], M. Ghaffari [c], M. Alizadeh [a], Ali K. Okyay [c]

[a] Department of Materials Science and Engineering, Shiraz University of Technology, 71555-313 Shiraz, Iran
[b] Department of Materials Science and Engineering, Semnan University, 3513119111 Semnan, Iran
[c] Department of Electrical and Electronics Engineering, UNAM-Institute of Materials Science and Nanotechnology, Bilkent University, Ankara 06800, Turkey

ARTICLE INFO

Article history:
Received 17 August 2012
Received in revised form 29 December 2012
Accepted 13 March 2013
Available online 10 April 2013

Keywords:
Nanocrystalline/amorphous materials
Shape memory alloys
Crystal structure
Microstructure
Phase transformation

ABSTRACT

The formation mechanism of Cu–11.5Al–4Mn alloys by mechanical alloying (MA) of pure elemental powders was investigated. During milling, the powder sampling was conducted at predetermined intervals from 1 h to 96 h. The quantitative phase analyses were done by X-ray diffraction and the particles size and morphology were studied by scanning electron microscopy. Furthermore, the microstructure investigation and phase identification were done by transmission electron microscopy. Concerning the results, the nanocrystalline Cu solid solution were formed at short milling times and, by milling evolution, the austenite-to-martensite (2H) phase transformation occurred. Moreover, the formation of considerable amount of amorphous phase and its partial transformation to crystalline phases during the milling process were revealed. It was also found that, by milling development, the powder morphology changes from lamellar to semi-spherical and their size initially increases, then reduces and afterward re-increases.

1. Introduction

Shape memory alloys (SMAs) are a class of advanced materials which exhibit superior properties such as shape memory effect (SME) and superelasticity (SE) due to reversible martensitic transformation [1–5]. Ni–Ti-based, Cu-based, and Fe-based alloys are important SMAs, which are widely used in aerospace applications, industrial safety, medical applications, civil engineering, and so on [1,5,6]. Among the alloys, Cu-based SMAs are less expensive than NiTi and have better SME and SE than Fe-based SMAs; consequently, they are the most attractive alloys for practical applications [7]. However, due to the high ordering degree and high elastic anisotropy in the β parent phase, the polycrystalline Cu-based SMAs particularly Cu–Zn–Al and Cu–Al–Ni are brittle to be sufficiently cold-worked [7,8]. Although some attempts have been made to improve the ductility of the SMAs (e.g. grain refinement) [7], there was limited success. According to Kainuma's findings [7,9,10], due to a decrease in the degree of ordering in the parent $L2_1$ phase [11], Cu–Al–Mn SMAs exhibit more ductility than Cu–Zn–Al and Cu–Al–Ni alloys. Alternatively, because of the difficulty of the stress concentration relaxation in the grain boundaries, the poor fracture and fatigue characteristics are also appeared in the alloys which are improved considerably by grain refining to nano-size levels [1]. Accordingly, it can be inferred that the synthesis and characterization of nanocrystalline CuAlMn SMAs are much more attractive for future works.

In these shape memory alloys the disordered β-phase is the stable phase at high temperatures and it transforms to the martensitic phase after quenching. However, the phase stability can be significantly altered by variation of the alloying elements fraction; for instance, by increasing the Al and Mn content in CuAlMn SMAs, the predominant martensite phase, the stability temperature range of the β phase, and the transformation temperatures can be changed considerably [12–14]. That is, the careful chemical composition control is very crucial in these alloying systems and more attention is required during the processing routes.

Although Cu-based SMAs are usually produced by induction melting, the optimization of microstructure and chemical composition in the method is quite difficult with respect to solid state routes such as mechanical alloying [15]. Among the mechanical alloying routes, ball milling process is one of the most common methods in which the powder particles are subjected to repeated cold welding, fragmenting and re-welding, causing an atomic scale alloying [16–18]. By using the MA process, not only the control of microstructure and chemical composition homogeneity is feasible,

* Corresponding author. Tel.: +98 711 7354500; fax: +98 711 7354520.
E-mail address: amini@sutech.ac.ir (R. Amini).

0921-8831/$ - see front matter © 2013 The Society of Powder Technology Japan. Published by Elsevier B.V. and The Society of Powder Technology Japan. All rights reserved.
http://dx.doi.org/10.1016/j.apt.2013.03.005

but also the formation of non-equilibrium phases such as nanocrystalline/amorphous phases, intermetallic phases, and supersaturated solid solutions is achievable [17–22].

According to the literature, the MA method was successfully used to synthesized Cu-based SMAs; for instance, Xiao Zhu and his co-workers [23], have reported the formation of Cu–Al–Ni SMA after 25 h ball milling. To the best of our knowledge, in the case of CuAlMn, there exist limited studies and the only work was recently done by Rezvani and Shokuhfar [24] on the qualitative phase analysis of the Cu–12.5Al–5Mn alloy synthesized by MA. In the report, pre-alloyed single phase CuAlMn solid solution was successfully prepared by MA. However, no systematic work is presented on the phase transformation, martensite formation and amorphization of this alloying system during MA. Furthermore, the quantitative phase analysis has not been reported in the alloying system. In the present study, the nanocrystalline/amorphous Cu–11.5Al–4Mn alloy with dominant 2H-martensite structure was successfully synthesized by MA and afterward the structural and microstructural evolution during the milling cycle was studied quantitatively.

2. Experimental procedure

In this study, Cu–11.5Al–4Mn SMAs were successfully produced by mechanical alloying (MA) of high purity (>99.5%) elemental Cu, Al and Mn powders (Merck Specification with particle sizes between 500 and 600 μm). The milling process was conducted in a planetary ball mill (Sepahan 84 D) with the tempered steel vials (capacity = 90 ml) and balls (4 balls of 20 mm diameter and 8 balls of 10 mm diameter). To prevent oxidation of the mixture, the sealed vials were evacuated and then filled with argon gas. A rotation speed of 450 rpm and the ball-to-powder weight ratio (BPR) of 20:1 were utilized.

The chemical composition of the alloyed powders was estimated by X-ray fluorescence analyzer (XRF, PHILIPS, PW2400) and inductively coupled plasma mass spectrometer (ICP-MS, Perkin-Elmer Sciex ELAN 6000). The morphology and size distribution of the powder particles were investigated by a scanning electron microscope (SEM, FEI, Nova Nanosem 430) and image analyzer (Dewinter Material Plus Software). Moreover, the structural properties of the as-milled powders were studied by powder

Table 1
The chemical composition of the 96 h milled powders.

Weight percent (%)										
Milling time (h)	Cu		Al		Mn		Fe		Cr	
	Con	AE	Con	AE	Con	AE	Con	AE	Con	AE
96	84.78	0.05	11.38	0.03	3.84	0.02	0.08	0.002	0.02	0.001

Con: concentration, AE: absolute error.

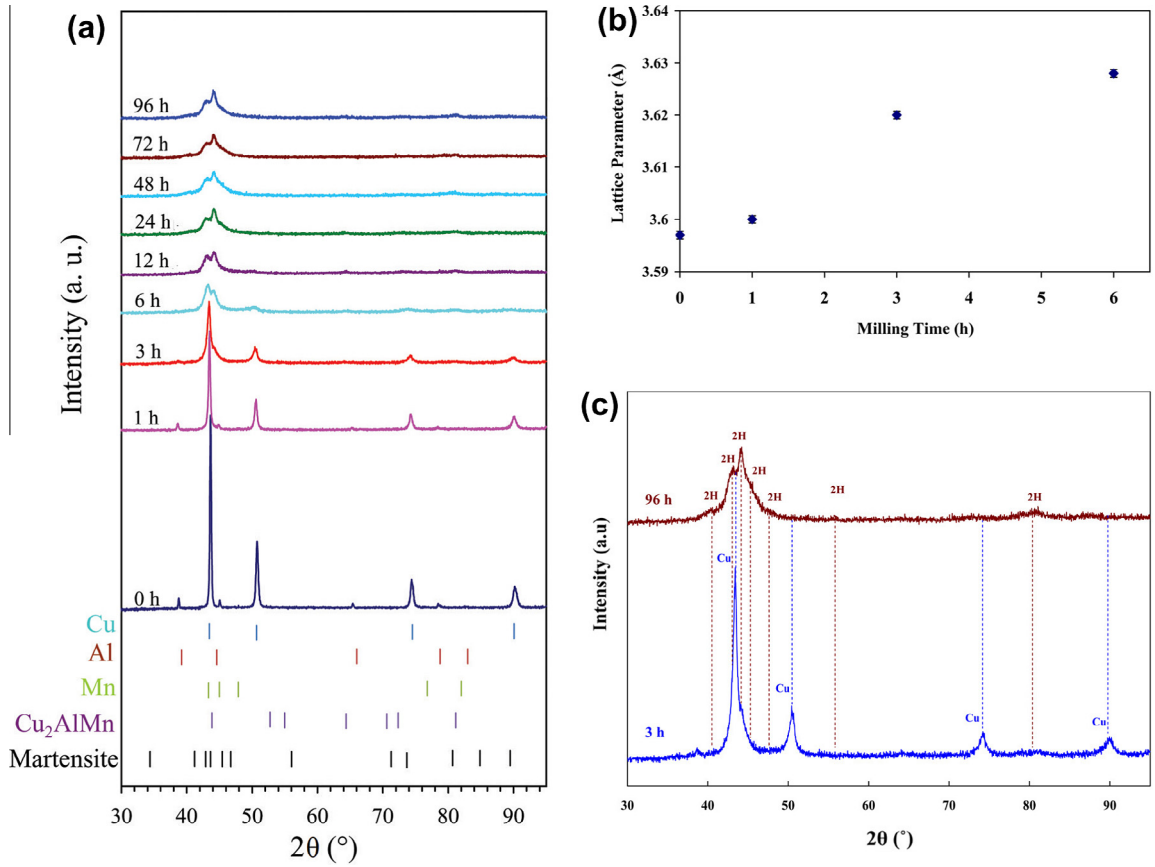

Fig. 1. (a) XRD patterns of the as-milled powders at different milling times, (b) variations of lattice parameter vs. milling time, and (c) the comparison of the XRD profiles of 3 h and 96 h milled powders.

X-ray diffraction (XRD, Pananalytical, X'pert Pro MPD,) with the Cu $K\alpha_{1,2}$ radiations, 2θ range of 30°–95°, step size of 0.03° and integration time of 6 s/step. The X-ray tube was operated at 40 kV and 40 mA. The quantitative phase analysis was done by Rietveld refinement of the XRD results using the MAUD software package version 2.33. The average crystallite size and microstrain of the as-milled powders were estimated by the Double-Voigt approach. The amorphous fraction was derived from an overestimation of an internal crystalline standard (in this work Zn powder with a median crystallite size of 60 nm) in an appropriate mixture of the standard and alloyed powders [25–28].

Eventually, in order to study the microstructural features of the alloyed powders and to confine the structural results, by transmission electron microscope (HRTEM, FEI, 2Tecnai G2 F30) the selected powders were dispersed in ethanol, dropped down to a copper grid, and subsequently characterized.

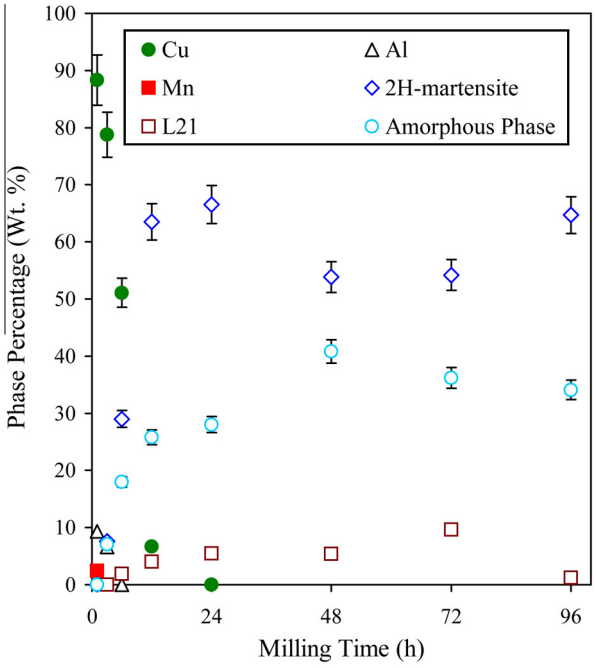

Fig. 2. The quantity variations of crystalline and amorphous phases by milling time.

3. Results and discussion

3.1. Chemical composition assessment

During the milling cycle, impurity incoming from the milling media to the as-milled powders may cause a deviation in the compound stoichiometry, provided that the milling conditions are not controlled correctly. Accordingly, chemical composition assessment during the milling process is very critical. Table 1 shows the chemical composition of the 96 h milled powders in which the expected nominal composition of Cu–11.5Al–4Mn is achieved even after prolonged milling times and the amount of impurities from the milling media (Fe and Cr) is negligible.

3.2. Phase evolution

Fig. 1a indicates the XRD patterns of the alloyed powders as a function of milling time. According to the results, by starting the milling process, the Al and Mn peaks diminish and eventually disappear and because of the development of nanosize structures and introduction of high amount of lattice strain, the Cu peaks are broadened considerably. At this stage, due to diffusion of Mn and Al elements into Cu structure, the Cu lattice parameter increases and its peaks position moves toward lower angles (Fig. 1b). By milling development, it can be seen that besides the Cu main peak, a new peak possibly corresponding to the 2H-martensite phase appears in the XRD profiles and, by further milling, the Cu-austenite peaks vanish and the martensite peak intensity increases (Fig. 1c). That is, due to severe plastic deformation and consequently

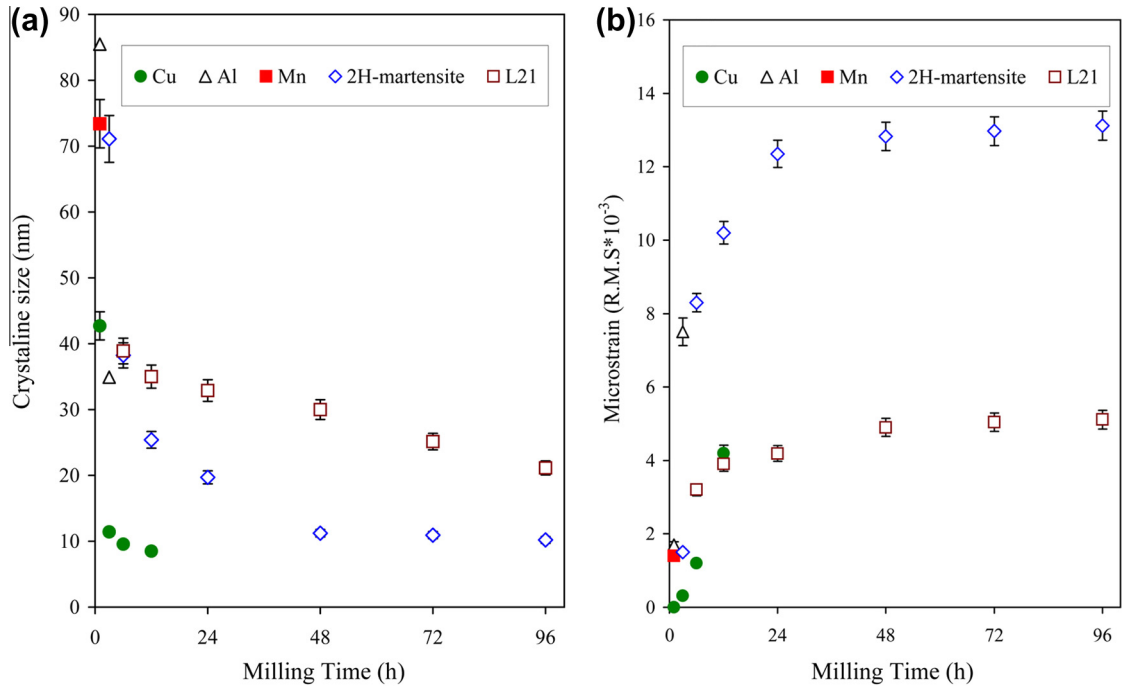

Fig. 3. The variations of (a) crystallite size and (b) microstrain of the different crystalline phases by milling time (determined by interpretation of the XRD results).

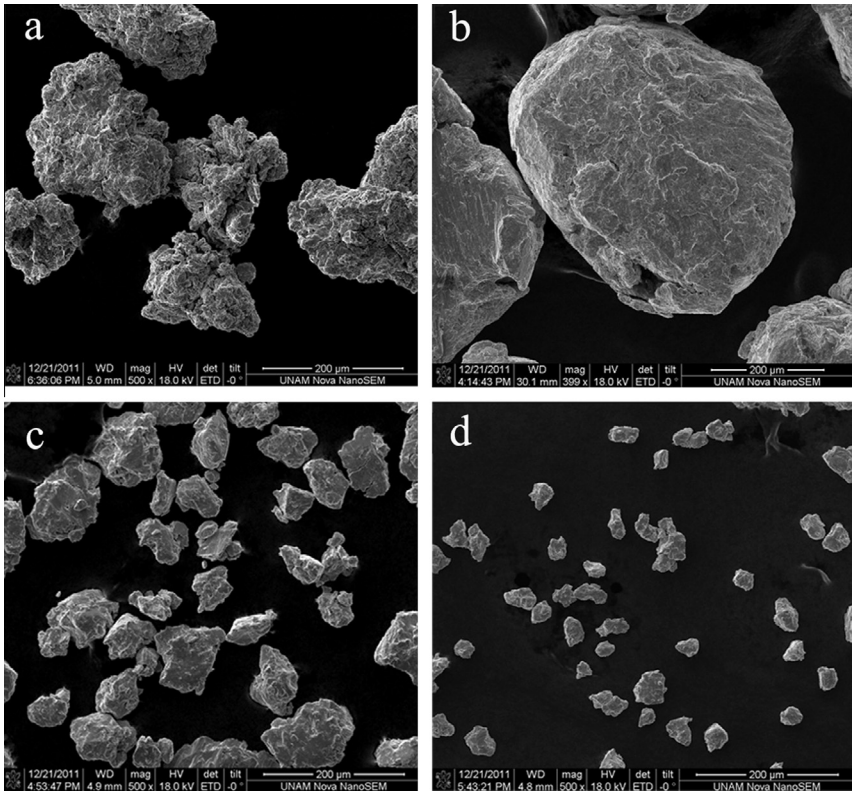

Fig. 4. The microstructural and morphological evaluation of the alloyed powders at various milling times. (a) 1 h; (b) 6 h; (c) 12 h; (d) 48 h.

Table 2
The average particle size and particle size distribution at different milling times.

Milling time (h)	Average particle size (μm)	Particle size distribution (μm)
1	180	145–215
3	280	200–320
6	500	400–600
12	140	110–170
24	94	74–107
48	38	28–52
96	40	31–56

significant stress introduction in the lattice, the transformation of austenite-to-the stress induced martensite occurred.

The quantity variations of the different phases at various milling times are illustrated in Fig. 2. As it can be seen, by starting the milling process, due to dissolution of Al and Mn in the structure, their weight fraction is reduced significantly and after 3 h of milling the dominant crystalline phase is Cu solid solution. It should be noticed that, owing to severe plastic deformation during milling, about 7 wt.% amorphous phase is also created at this time interval. By milling to 6 h, the percentage of amorphous phase increases to about 18 wt.% and due to the austenite-to-martensite phase transformation, a considerable amount of 2H-martensite phase is also created (29 wt.%) besides the Cu solid solution. Moreover, because of temperature increase during the milling process, the low quantity (about 2 wt.%) of high temperature $L2_1$ phase was also created during the milling cycle. By milling development to 24 h, total dissolution of Cu solid solution occurred and the amount of amorphous, 2H, and $L2_1$ phases increases to almost 28 wt.%, 66 wt.%, and 6 wt.% respectively. Milling evolution to 48 h resulted in the 2H reduction and amorphous phase increasing without any detectable change in the $L2_1$ quantity. That is, the transformation of 2H-to-amorphous phase occurs whenever the free energy of the 2H-martensite phase sufficiently exceeds that of the amorphous phase. This is due to high structural defects introduced into the 2H-phase structure during milling. The results of 72 h milled samples reveal that at the time intervals of 48–72 h, possibly due to temperature increasing during MA, the mechano-crystallization of the amorphous phase to the more stable $L2_1$ phase occurred and the amorphous amount reduced from 41 wt.% to 36 wt.%. As it is appeared, at the moment, the amount of 2H is approximately constant. Finally, it can be seen that by milling progression to 96 h, the amount of $L2_1$ reduced significantly

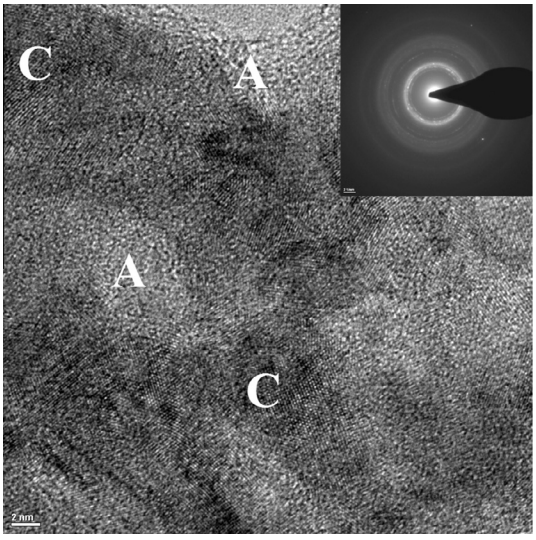

Fig. 5. The HRTEM image and the corresponding selected area diffraction pattern of 96 h milled powders.

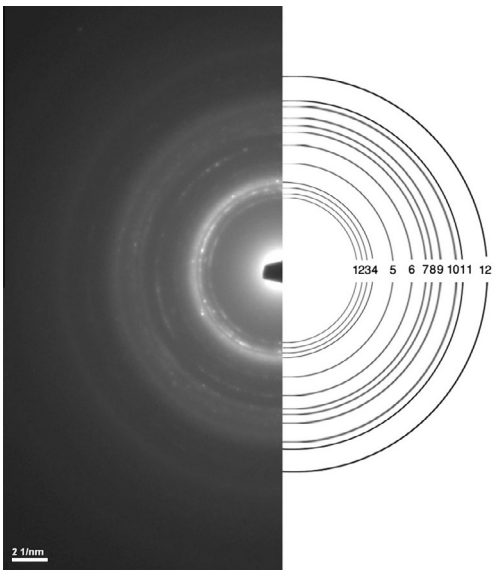

circle	d.spacing	(h k l)	phase
1	2.63	(1 1 1)	2H
2	2.28	(1 2 0)	2H
3	2.19	(2 0 0)	2H
4	2.11	(0 0 2)	2H
4	2.07	(2 2 0)	$L2_1$
4	2.08	(2 1 0)	2H
4	2.01	(1 2 1)	2H
5	1.94	(2 0 1)	2H
6	1.64	(0 3 1)	2H
7	1.52	(2 0 2)	2H
8	1.32	(3 1 1)	2H
9	1.28	(3 2 0)	2H
10	1.19	(1 2 3)	2H
10	1.14	(2 4 0)	2H
11	1.09	(3 2 2)	2H
12	0.94	(1 4 3)	2H

Fig. 6. The reflection rings origin of the SAD pattern of Fig. 5.

and the quantity of 2H is re-increased. It can be attributed to the formation of stacking faults and also the stresses introduction due to severe plastic deformation during the milling cycle [29].

The aforementioned results indicate that the thermodynamic state of the existing phases has a crucial role in the phase stability during MA. Consequently, depending on the phase stability, different and rarely inverse phase transitions can occur at various milling intervals.

The variation of crystallite size and microstrain of the present crystalline phases by milling evolution is depicted in Fig. 3. As it is evident, the nanocrystallization was developed at short milling times and the reduction in crystallite size occurred rapidly and then was continued gradually. Furthermore, it can be seen that as a result of severe collisions between the powder particles and milling media, the crystalline defects and consequently the lattice strains increase considerably by milling progression.

3.3. SEM observations

The microstructural and morphological variations of the as-milled powders are shown in the SEM micrograph of Fig. 4. Also, the average particle size and particle size distribution at different milling time are listed in Table 2. Concerning the results, at early stage of milling time (1 h) the powders are highly agglomerated, their morphology is irregular, and the average particle size is about 180 μm. By continuation of milling (6 h), because of the ductile nature of the constituent elements, the severe cold welding occurred and the particle size is severely increased to 500 μm with a wide particle size distribution of 400–600 μm. By further milling, due to high energy collisions between the milling media and the powder particles, the cold welded particles are fragmented and their average size and size distribution are subsequently reduced considerably. Austenite-to-martensite phase transformation is also enhanced the phenomenon. By milling evolution, parallel to enhancement of more brittle amorphous phase, the reduction of size distribution and average particle size is continued and their morphology turns into the equiaxed.

3.4. TEM studies

Fig. 5 demonstrates the high resolution TEM (HRTEM) image and the corresponding selected area diffraction (SAD) pattern of the 96 h milled powders. Concerning the figure, a combination of crystalline and amorphous phases is appeared in the HRTEM image which is confirmed by the continuous crystalline rings and amorphous halo pattern of the correlated SAD. In order to verify the origin of reflection rings, the SAD pattern of the 96 h powders was interpreted and the results were depicted in Fig. 6. According to the results, most of the crystalline rings are related to the 2H-martensite structure, verifying the XRD results.

4. Conclusions

In the present work, the nanocrystalline/amorphous Cu–11.5Al–4Mn alloys were successfully synthesized by mechanical alloying of pure elemental powders and their structural and microstructural evolution during the milling process was studied. Concerning the results, it can be inferred that:

(1) During milling, the reduction in crystallite size to nanometric levels and the increase in the lattice strain rapidly occurred and then were gradually sustained.
(2) By milling initiation, the elemental powders were becoming dissolved into the structure and after short milling times, the formation of supersaturated solid solution of Al and Mn in Cu was indicated.
(3) By milling progression, the austenite-to-martensite (2H) phase transformation occurred and a significant amount of amorphous phase was also formed.
(4) By further milling, the amount of the amorphous phase was increased considerably and the partial amorphization of 2H-martensite phase happened.
(5) After sufficient milling time, the mechano-crystallization of the amorphous phase to more stable $L2_1$ phase occurred and its amount was reduced by milling development.
(6) At the end of milling, the transformation of $L2_1$ to 2H martensite phase occurred and consequently the fraction of 2H was re-increased.
(7) By milling development, the particles morphology was changed from plate-like to semi-sphere and then to irregular shapes. Furthermore, the average particles size was initially increased, then reduced, and subsequently re-increased.

Acknowledgements

Parts of this work were supported by EU FP7 Marie Curie IRG Grant 239444, COST NanoTP, TUBITAK Grants 108E163, 109E044 and 112M004.

References

[1] K. Otsuka, in: C.M. Wayman (Ed.), Shape Memory Materials, Cambridge University, Cambridge, 1998. pp. 1–27.
[2] O. Adigüzel, Martensite ordering and stabilization in copper based shape memory alloys, Mater. Res. Bull. 30 (1995) 755–760.
[3] D.D. Radev, Mechanical synthesis of nanostructured titanium–nickel alloys, Adv. Powder Technol. 21 (2010) 477–482.
[4] F.J. Gil, J.M. Guilemany, The Determination of the electron to atom ratio interval corresponding to the change in the martensitic structure from α′ to β′ in Cu–Zn–Al shape memory alloys, Mater. Res. Bull. 27 (1992) 117–122.
[5] C. Cismasiu, Shape Memory Alloys, Sciyo, Croatia, 2010.
[6] M. Schwartz, Encyclopedia of Smart Materials, John Wiley and Sons, New York, 2002.
[7] Y. Sutou, T. Omori, J.J. Wang, R. Kainuma, K. Ishida, Characteristics of Cu–Al–Mn-based shape memory alloys and their applications, Mater. Sci. Eng. A 378 (2004) 278–282.
[8] J.I. Pérez-Landázbal, V. Recarte, V. Sónchez-Alarcos, M.L. Nó, J.S. Juan, Study of the stability and decomposition process of the β phase in Cu–Al–Ni shape memory alloys, Mater. Sci. Eng. A 438–440 (2006) 734–737.
[9] R. Kainuma, S. Takahashi, K. Ishida, Thermoelastic martensite and shape memory effect in ductile Cu–Al–Mn alloys, Metall. Mater. Trans. A 27A (1996) 2187–2195.
[10] R. Kainuma, S. Takahashi, K. Ishida, Ductileshapememoryalloy of the Cu–Al–Mn system, J. Phys. IV 5 (C8) (1995) 961–966.
[11] Y. Sutou, N. Koeda, T. Omori, R. Kainuma, K. Ishida, Effects of ageing on bainitic and thermally induced martensitic transformations in ductile Cu–Al–Mn-based shape memory alloys, Acta. Mater. 57 (2009) 5748–5758.
[12] R. Kainuma, N. Satoh, X.J. Liu, I. Ohnuma, K. Ishida, Phase equilibria and Heusler phase stability in the Cu-rich portion of the Cu–Al–Mn system, J. Alloys Compd. 266 (1998) 191–200.
[13] U. Sarı, İ. Aksoy, Electron microscopy study of 2H and 18R martensites in Cu–11.92 wt% Al–3.78 wt% Ni shape memory alloy, J. Alloys Compd. 417 (2006) 138–142.
[14] A. Ibarra, J.S. Juan, E.H. Bocanegra, M.L. Nõ, Thermo-mechanical characterization of Cu–Al–Ni shape memory alloys elaborated by powder metallurgy, Mater. Sci. Eng. A 438–440 (2006) 782–786.
[15] Z. Li, Z.Y. Pan, N. Tang, Y.B. Jiang, N. Liu, M. Fang, F. Zheng, Cu–Al–Ni–Mn shape memory alloy processed by mechanical alloying and powder metallurgy, Mater. Sci. Eng. A 417 (2006) 225–229.
[16] M.Sh. El-Eskandarany, Mechanical Alloying for Fabrication of Advanced Engineering Materials, Al Azhar University, Noyes, Cairo, 2001.
[17] C. Suryanarayana, Mechanical Alloying and Milling, Marcel Dekker, New York, 2004.
[18] C. Suryanarayana, Recent developments in mechanical alloying, Rev. Adv. Mater. Sci. 18 (2008) 203–211.
[19] Z. Adabavazeh, F. Karimzadeh, M.H. Enayati, Synthesis and structural characterization of nanocrystalline (Ni, Fe)3Al intermetallic compound prepared by mechanical alloying, Adv. Powder Technol. 23 (2012) 284–289.
[20] E. Salahinejad, R. Amini, M.J. Hadianfard, Structural evolution during mechanical alloying of stainless steels under nitrogen, Powder Technol. 215–216 (2012) 247–253.
[21] Z. Zhang, R. Sandström, K. Frisk, A. Salwén, Characterization of intermetallic Fe–Mn–Si powders produced by casting and mechanical ball milling, Powder Technol. 137 (2003) 139–147.
[22] G.H. Xu, K.F. Zhang, Z.Q. Huang, The synthesis and characterization of ultrafine grain NiAl intermetallic, Adv. Powder Technol. 23 (2012) 366–371.
[23] X. Zhu, I. Zhou, L. Ming, T. Ning, Structure evolution of Cu-based shape memory powder during mechanical alloying, Trans. Nonferrous Met. Soc. China 17 (2007) 1422–1427.
[24] M.R. Rezvani, A. Shokuhfar, Synthesis and characterization of nanostructured Cu–Al–Mn shape memory alloy by mechanical alloying, Mater. Sci. Eng. A 532 (2012) 282–286.
[25] R.S. Winburn, D.G. Grier, G.J. Mccarthy, R.B. Peterson, Rietveld quantitative X-ray diffraction analysis of NIST fly ash standard reference materials, Powder Diffr. 15 (2000) 163–172.
[26] A.G. De La Torre, S. Bruque, M.A.G. Aranda, Rietveld quantitative amorphous content analysis, J. Appl. Cryst. 34 (2001) 196–202.
[27] S. Kemethmüller, A. Roosen, F. Goetz-Neunhoeffer, J. Neubauer, Quantitative analysis of crystalline and amorphous phases in glass–ceramic composites like LTCC by the Rietveld method, J. Am. Ceram. Soc. 89 (2006) 2632–2637.
[28] P.S. Whitfield, L.D. Mitchell, Quantitative Rietveld analysis of the amorphous content in cements and clinkers, J. Mater. Sci. 38 (2003) 4415–4421.
[29] Y. Zhang, N.R. Tao, K. Lu, Effects of stacking fault energy, strain rate and temperature on microstructure and strength of nanostructured Cu–Al alloys subjected to plastic deformation, Acta. Mater. 59 (2011) 6048–6058.